# Elastic properties of perovskite $YCrO_3$ up to 60 GPa

M. Ardit and G. Cruciani*
*Earth Science Department, University of Ferrara, 44100 Ferrara, Italy*

M. Dondi
*Institute of Science and Technology for Ceramics (ISTEC)-CNR, 48018 Faenza, Italy*

M. Merlini
*Earth Science Department, University of Milano, 20133 Milano, Italy*

P. Bouvier
*Laboratoire des Matériaux et du Génie Physique, CNRS-Grenoble Institute of Technology, 38016 Grenoble, France and European Synchrotron Radiation Facility, BP 220, F-38043 Grenoble Cedex, France*
(Received 16 April 2010; published 20 August 2010)

The high-pressure evolution of the $YCrO_3$ perovskite structure (space group *Pbnm*) has been investigated using synchrotron powder diffraction, up to 60 GPa. The results show an anisotropy in the elastic moduli of the individual crystallographic axes: the *b* axis is appreciably less compressible than both *a* and *c* axes [$K_{a0}$=195(5) GPa, $K_{b0}$=223(7) GPa, and $K_{c0}$=200(6) GPa, respectively]. This implies that $YCrO_3$ becomes more distorted with increasing pressure, which is similar to what was previously found in $YTiO_3$ but opposite to the behavior reported for $YAlO_3$. Such contrasting trends are explained by the stronger confinement of Y ions in $YAlO_3$ due to the smaller size of octahedral network in the orthoaluminate compared to the orthochromate.

DOI: 10.1103/PhysRevB.82.064109 PACS number(s): 62.20.de, 61.50.Ks, 91.60.Ba, 61.05.cp

## I. INTRODUCTION

Perovskites are ternary compounds with general formula $^{[XII]}A\,^{[VI]}BO_3$. Their ideal crystal structure is cubic (*Pm*-3*m* symmetry) and made by a framework of corner-sharing octahedra hosting the *B* cations while the *A* cations are placed in the resulting extra-framework dodecahedral sites. Variations in the chemical nature of *A* and *B* cations, as well as changes in pressure and temperature, are accommodated by octahedral tilting distortions which lower the real symmetry and control the physical properties of these materials.[1]

Perovskites are of great interest in Earth sciences because, at the high pressure and temperature conditions of the Earth's lower mantle, the pyroxene enstatite, $MgSiO_3$, transforms into a denser perovskite-structured polymorph.[2]

The group of 3:3 perovskites (trivalent cations in both *A* and *B* sites) has gained much interest in several technological fields due to their peculiar electric, magnetic, piezoelectric, and optical properties.[3,4] Industrial applications of the $YCrO_3$ perovskite, subject of this study, include its use as interconnection for the solid oxide fuel cells[5] while in pure science it has been applied to develop model for defective structures.[6]

Furthermore, its multifunctional biferroic behavior (i.e., possessing both ferromagnetic and ferroelectric properties) has been reported and explained by a local noncentrosymmetry arising from ~0.01 Å displacement of $Cr^{3+}$ ions along the *c* axis with respect to the center of *B* octahedra.[7] The orthorhombic symmetry is maintained for the average crystallographic structure.[8]

A recent work established the structural relaxation along the $YAlO_3$-$YCrO_3$ join.[9] Compared to garnet, spinel, and corundum, the lowest relaxation around $Cr^{3+}$ found in perovskite was in contrast with the lattice flexibility expected on the basis of its corner-sharing octahedral framework. Possible explanations involved the role of covalency in Cr-O bonds or the different elastic properties of the two end members.

In the last decade, many studies have been devoted to assess the high-pressure behavior of both 2:4 and 3:3 orthorhombic perovskites,[10–23] and a general rule has been formulated.[18] It predicts that at high pressures the octahedral tilting and perovskite distortion will increase in the 2:4 group (e.g., $CaTiO_3$) and decrease in the 3:3 group of perovskites (e.g., $YAlO_3$). No data have been reported so far on the high-pressure behavior of $YCrO_3$ belonging to the 3:3 group.

This study is aimed at determining the elastic properties of the orthochromate perovskite up to 60 GPa by means of *in situ* synchrotron powder diffraction. Comparison with the high-pressure behavior of orthoaluminate will help to understand the low relaxation around $Cr^{3+}$ in the $YAlO_3$-$YCrO_3$ perovskite system.

## II. EXPERIMENTAL PROCEDURE

### A. Sample preparation

The $YCrO_3$ perovskite sample was synthesized via solid-state reaction by using reagent-grade $Y_2O_3$ and $Cr_2O_3$ (>99% of purity) as precursors. The raw materials were mixed and homogenized by ball milling in acetone, then oven dried at 100 °C. Dry powders were calcined in an electric kiln at 1300 °C for several hours, in static air and unsealed alumina crucible.

### B. Synchrotron x-ray diffraction

High-pressure x-ray powder-diffraction data were collected *in situ* at the ID27 beamline (ESRF, Grenoble). Both,

 

the sample and the ruby grain for pressure calibration were loaded into a membrane type diamond-anvil cell, with the gasket filled with helium as pressure-transmitting medium in order to achieve quasihydrostatic pressure conditions.[24] Diffraction patterns were collected using monochromatic x rays ($\lambda$=0.3738 Å) at room temperature, and both the sample-to-detector distance and detector tilt were calibrated using silicon. The pressure cell was allowed to relax for several minutes at each pressure. All patterns, collected till a maximum pressure of 60.4 GPa on a Mar245 charge coupled device detector, were integrated over the full rings using the FIT2D program,[25] masking all the diffraction peaks of diamond and solid He, in order to obtain the conventional intensity versus $2\theta$ step angle patterns. The intensity variation along each diffraction ring was used to estimate the statistical error of step counts. As mentioned above, the pressure was measured using the ruby fluorescent method,[26] with estimated precision of $\pm$0.05 GPa for the measured pressures.

### C. Rietveld refinements

The collected data have been modeled by the Rietveld method using the GSAS-EXPGUI software packages.[27,28] The structure refinement of $YCrO_3$ orthorhombic perovskite was carried out in the *Pbnm* space group, starting from the atomic parameters of $YAlO_3$,[29] with Cr replacing Al. The diffraction peak profile was modeled by a pseudo-Voigt function with one Gaussian and one Lorentzian broadening coefficients. Besides the 15 shifted Chebyshev polynomial coefficients to reproduce the background, the refinement included a scale factor, the cell parameters, and the atomic coordinates. Two representative Rietveld plots at low (4.6 GPa) and high (42.6 GPa) pressure are given in Fig. 1. Refined unit-cell parameters, final atomic coordinates, and isotropic atomic displacement parameters of $YCrO_3$ perovskite at ambient pressure,[9] 4.6 and 42.6 GPa are reported in Table I.

Previously reported crystal structure determinations of $YCrO_3$ (at ambient conditions) include an early model with not refined atomic coordinates,[30] and the more recent study by Ramesha *et al.*[8] using neutron powder diffraction and pair distribution function analysis. The results of our structure refinement at room pressure are identical, within the standard error, to those obtained from the latter study (see Table II for comparison).

## III. RESULTS AND DISCUSSION

### A. Elastic properties of $YCrO_3$

The pressure dependence of the unit-cell volume of $YCrO_3$ perovskite is plotted in Fig. 2. The volume reduction is about 17.5% in the studied pressure range. No evidences for phase transitions were found up to 60.4 GPa.

The *P-V* data, fitted with a third-order Birch-Murnagham equation of state (EoS) [Eq. (1)],

$$P = \frac{3K_{T0}}{2}\left[\left(\frac{V_0}{V}\right)^{7/3} - \left(\frac{V_0}{V}\right)^{5/3}\right] \times\left\{1 + \frac{3}{4}(K_0' - 4)\cdot\left[\left(\frac{V_0}{V}\right)^{2/3} - 1\right]\right\} \quad (1)$$

give a $V_0$=218.23(4) Å$^3$, equal to the value obtained for the same sample refined at room pressure,[9] and to a volumetric bulk modulus $K_{T0}$=208.4(5) GPa with a $K_0'$=3.7(1).

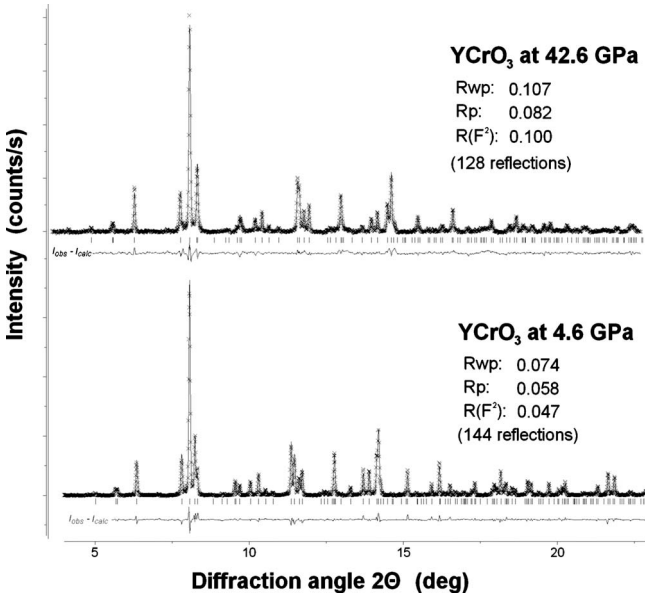


FIG. 1. Plot of the Rietveld refinements for $YCrO_3$ at 4.6 GPa (at the bottom) and 42.6 GPa (on the top) at room temperature ($\lambda$ =0.3738 Å). The experimental data are indicated by crosses, the calculated pattern is the continuous line, whereas the lower curve is the weighted difference between the observed and calculated patterns. Vertical ticks mark the position of reflections for $YCrO_3$ in the *Pbnm* space group.

Normalized stress-strain (*F-f*) plot (Fig. 3) provides a visual indication of how the $K_0'$ term is significant in the EoS fitting.[32] If the EoS was truncated at second order all data points could lie on a horizontal line of constant $F$ ($K_0'$=4),

TABLE I. Unit-cell parameters, final atomic coordinates, and isotropic atomic displacement parameters of $YCrO_3$ perovskite at ambient pressure (Ref. 9), 4.6 and 42.6 GPa. Fixed coordinates: $z_Y=\frac{1}{4}$; $x_{Cr}=0$, $y_{Cr}=z_{Cr}=\frac{1}{2}$; $z_{O1}=\frac{1}{4}$.

| | $P$=0 GPa | $P$=4.6 GPa | $P$=42.6 GPa |
|---|---|---|---|
| $a$ (Å) | 5.2434(1) | 5.2028(1) | 4.9403(2) |
| $b$ (Å) | 5.5242(1) | 5.4872(1) | 5.2767(2) |
| $c$ (Å) | 7.5356(1) | 7.4808(1) | 7.1995(2) |
| Volume (Å$^3$) | 218.27(1) | 213.57(1) | 187.16(1) |
| $x_Y$ | −0.0167(2) | −0.0170(3) | −0.0205(5) |
| $y_Y$ | 0.0664(1) | 0.0673(2) | 0.0713(3) |
| $Ueq._Y$ (Å$^2\times$100) | 1.39(2) | 1.16(4) | 1.40(4) |
| $Ueq._{Cr}$ (Å$^2\times$100) | 1.26(4) | 1.05(10) | 1.33(9) |
| $x_{O1}$ | 0.101(1) | 0.097(1) | 0.105(2) |
| $y_{O1}$ | 0.465(1) | 0.458(1) | 0.470(2) |
| $Ueq._{O1}$ (Å$^2\times$100) | 1.7(2) | 1.8(4) | 1.6(4) |
| $x_{O2}$ | 0.693(1) | 0.679(1) | 0.686(2) |
| $y_{O2}$ | 0.302(1) | 0.297(1) | 0.299(2) |
| $z_{O2}$ | 0.055(1) | 0.055(1) | 0.053(1) |
| $Ueq._{O2}$ (Å$^2\times$100) | 1.6(1) | 1.5(3) | 1.5(3) |

TABLE II. Comparison of selected parameters for $YCrO_3$ models at ambient pressure. O2′ and O2″ coordinates obtained from O2 $(x,y,z)$ in Table I by the following relations: $x_{O2'}=\frac{1}{2}+x_{O2}$; $y_{O2'}=\frac{1}{2}-y_{O2}$; $z_{O2'}=\frac{1}{2}+z_{O2}$ and $x_{O2''}=1-x_{O2}$; $y_{O2''}=1-y_{O2}$; $z_{O2''}=\frac{1}{2}+z_{O2}$. $M_A/M_B$: ratio of total estimated variation in bond valence in a polyhedral site due to change in average bond distance (Refs. 18 and 19). $M_i=\frac{R_iN_i}{B}\exp(\frac{R_0-R_i}{B})$, where $R_i$=average bond length; $N_i$=coordination number of the cation site at ambient condition; $R_0$=bond valence parameter (Ref. 31); $B$=universal constant (0.37) (Ref. 31). $V_A$ and $V_B$=volumes of $A$ and $B$ polyhedra, respectively; superscript is the assumed coordination number.

| | $YCrO_3$ (Ref. 9) | $YCrO_3$ (Ref. 8) |
|---|---|---|
| $\langle^{VIII}$Y-O$\rangle$ (Å) | 2.417 | 2.415 |
| $\langle^{XII}$Y-O$\rangle$ (Å) | 2.738 | 2.735 |
| Cr-O1 (Å) | 1.967(2) | 1.971(1) |
| Cr-O2′ (Å) | 1.988(4) | 1.983(1) |
| Cr-O2″ (Å) | 1.998(4) | 1.993(1) |
| ⟨Cr-O⟩ (Å) | 1.984 | 1.982 |
| $M_A/M_B$ | 1.18 | 1.18 |
| $^{VIII}V_A$ (Å$^3$) | 23.52 | 23.44 |
| $^{XII}V_A$ (Å$^3$) | 46.18 | 46.05 |
| $^{VI}V_B$ (Å$^3$) | 10.40 | 10.37 |
| Cr-O1-Cr (deg) | 146.7(3) | 145.6(1) |
| Cr-O2-Cr (deg) | 145.7(2) | 146.3(1) |

whereas in the case of $YCrO_3$ the data lie on an inclined line, correctly described by a third-order truncation of the Birch-Murnagham EoS.

The elastic moduli of the individual crystallographic axes are obtained by fitting the measured data with the same EoS [Eq. (1)] to the cubes of each of the cell axes. The resulting axial moduli: $K_{a0}=195(5)$ GPa, $K_{b0}=223(7)$ GPa, and $K_{c0}=200(6)$ GPa, highlight how the $b$ axis is appreciably less compressible than both $a$ and $c$ axes, which have similar compressibilities (Fig. 4). The direct result is that the $YCrO_3$ perovskite structure becomes more distorted with increasing pressure.

Such a behavior is different compared to what was reported for the orthorhombic $YAlO_3$ perovskite in which the $b$ axis is significantly more compressible than both $a$ and $c$,

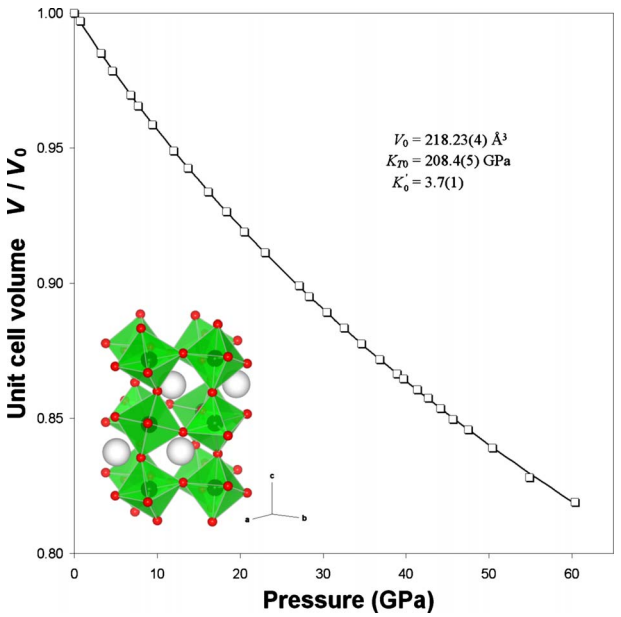


FIG. 2. (Color online) Variation in the unit-cell volume of $YCrO_3$ perovskite between room pressure and 60.4 GPa. The inset displays the structure of $YCrO_3$ perovskite along the [110]. Line refers to the EoS calculated value.

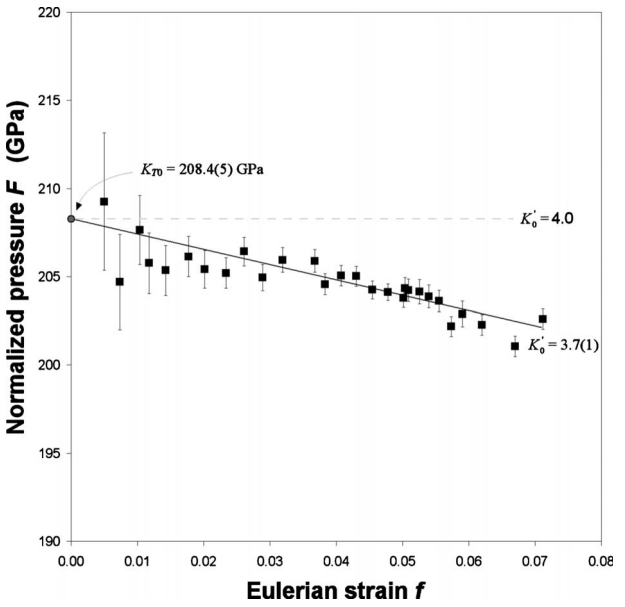


FIG. 3. Normalized stress-strain ($F$-$f$) plot derived from the measured volumes for a third-order Birch-Murnagham EoS. The normalized pressure stress $F$ is defined as $F=P/3f(1+2f)^{5/2}$ while the finite Eulerian strain $f$ is defined as $f=[(V_0/V)^{2/3}-1]/2$.

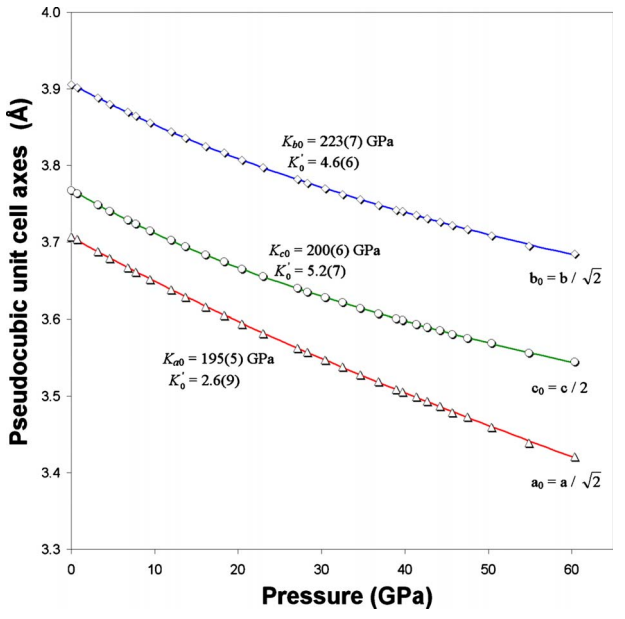


FIG. 4. (Color online) Variation in the pseudocubic unit-cell axes of $YCrO_3$ perovskite between room pressure and 60.4 GPa.

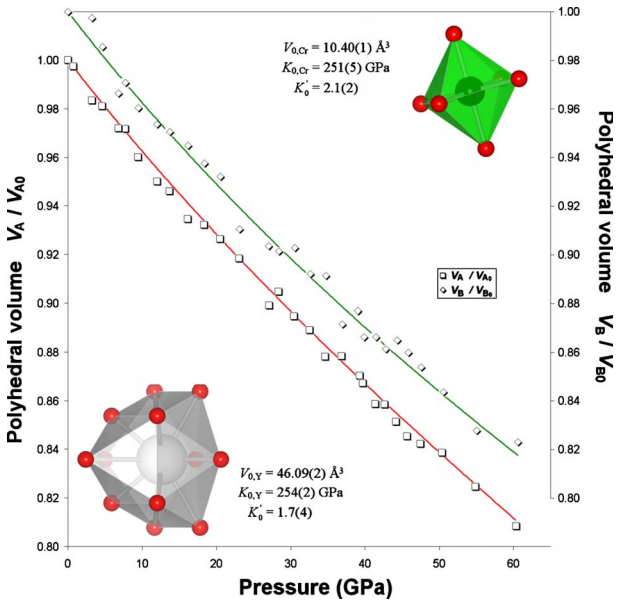


FIG. 5. (Color online) Variation in the polyhedral volume of $YCrO_3$ perovskite between room pressure and 60.4 GPa. Continuous lines define the EoS calculated to fit the data sets.

given the corresponding axial moduli: $K_{a0}$=219(7) GPa, $K_{b0}$=157(3) GPa, and $K_{c0}$=212(2) GPa.[17] Consequently the two structures show a different anisotropic behavior along [010] and [101].

The polyhedral bulk moduli for $YO_{12}$ and $CrO_6$ polyhedra (see Fig. 5 for pressure dependence) were calculated using the same formalism applied to fit the *P*-*V* data, obtaining $V_{0,poly}$, $K_{p0}$:46.09(2) Å$^3$, 254(2) GPa for $YO_{12}$, and 10.40(1) Å$^3$, 251(5) GPa for $CrO_6$. The volume compressibilities of the $YO_{12}$ and $CrO_6$ sites are therefore equivalent, whereas for the $YAlO_3$ perovskite the compressibility of the cubic site is ~15% less than that of the $AlO_6$ octahedron.[17]

Besides the overall polyhedral compression, information about pressure-driven electronic changes in transition-metal perovskites can be inferred from the changes in octahedral distortion as a function of pressure. For instance, the variation in Ti-O bond distances in $YTiO_3$ indicated the possibility of a pressure-induced spatial reorientation of the occupied $t_{2g}$ orbitals in $Ti^{3+}$ ions [electron configuration $3d^1(t_{2g})$].[21] Considering that $Cr^{3+}$ [configuration $3d^3(t_{2g})$] is also a non-Jahn-Teller ion, the pressure-driven orbital reorientation can be evaluated, in analogy to $YTiO_3$, by inspecting the changes in Cr-O bond lengths in the selected pressure range up to 35 GPa (Fig. 6).

The variation in Cr-O2′, Cr-O2″, and Cr-O1 distances, respectively, along the *x*, *y*, and *z* directions of the local coordinate system at Cr site, resembles very much what was found in $YTiO_3$. In both cases, at a given pressure (13 GPa for $YTiO_3$ and about 28 GPa for $YCrO_3$) two almost equal *B*-O2 and one shorter *B*-O1 distances occur, implying that the *B* octahedra are compressed along *z* and that the orbital reorientation has taken place. The distinct pressure of the orbital reorientation in $YTiO_3$ and $YCrO_3$ can be ascribed to

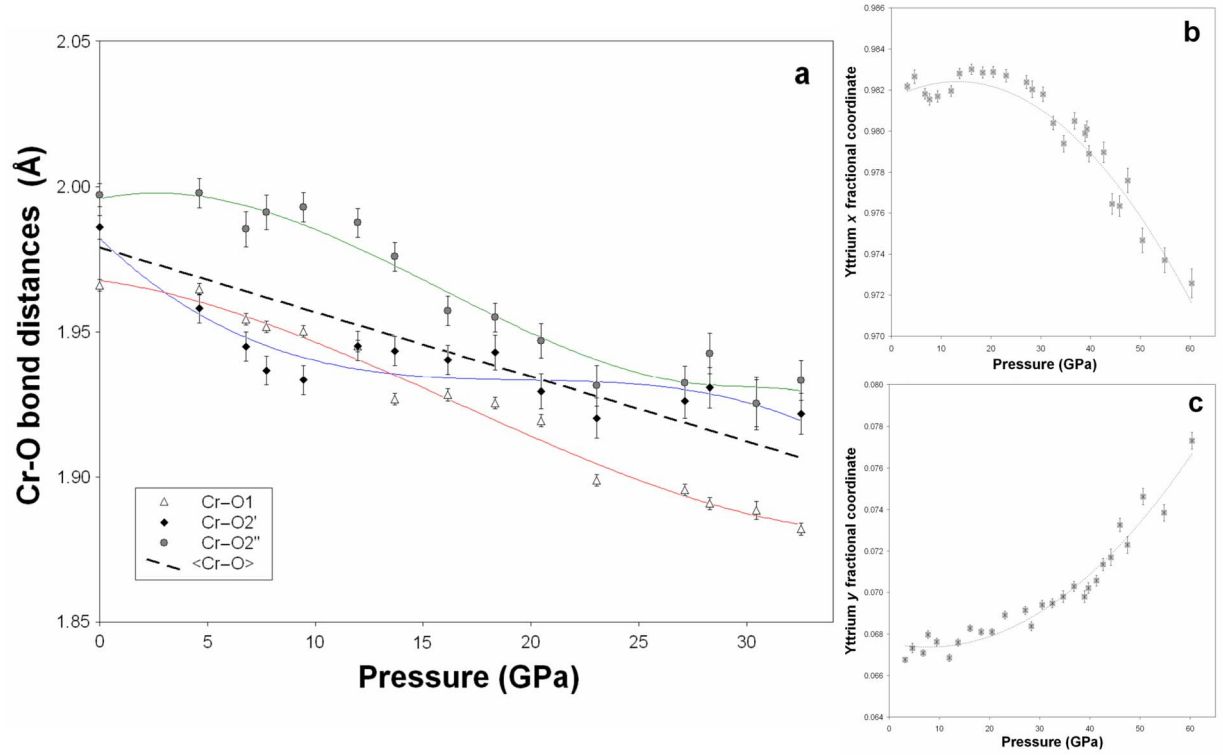


FIG. 6. (Color online) (a) Variation in the Cr-O bond lengths in $YCrO_3$ as a function of pressure up to 35 GPa. This upper limit is selected in order to evaluate the octahedral distortion as much as possible unaffected by the variations within the $YO_{12}$ polyhedra. In fact, the displacement of Y ions [*x* and *y* coordinates in (b) and (c), respectively] away from the center of the dodecahedron is very close to the initial value in the 0–35 GPa pressure range.

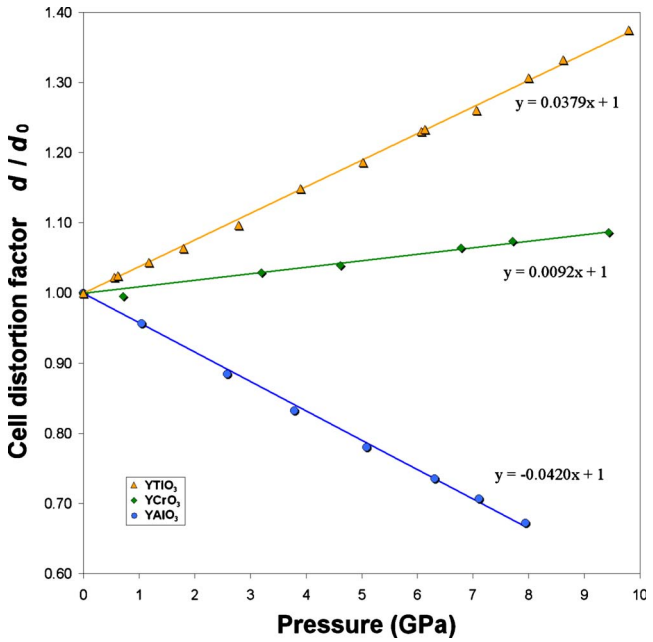


FIG. 7. (Color online) Cell distortion parameter $(d/d_0)$ of $YCrO_3$, $YCrO_3$, and $YAlO_3$ perovskites versus pressure.

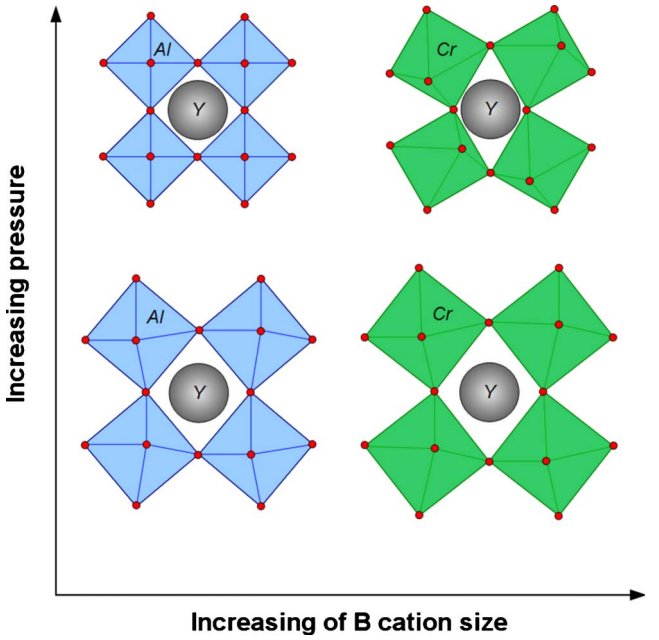


FIG. 8. (Color online) Sketch illustrating the effects of $B$ cation size and pressure on distortion of $YCrO_3$ and $YAlO_3$ perovskites. Actual differences in size and distortion are exaggerated for the sake of clarity.

the different electron configuration of the transition-metal ions and to the lattice elastic properties.

As far as the effects of pressure on the biferroic character of $YCrO_3$, given that it is caused by the off-center shift of Cr ions along the $z$ direction of octahedra, we expect that compression up to 28 GPa would also lead to disappearance of both the ferromagnetic and ferroelectric properties. Experimental confirmation of this suggestion needs further work which is beyond the scope of the present study.

### B. Pressure dependence of cell distortion

In order to better appreciate how the pressure influences the behavior of the three isotopic $YM^{3+}O_3$ ($M^{3+}$=$Cr^{3+}$, $Al^{3+}$, and $Ti^{3+}$) perovskites, the unit-cell parameters of $YCrO_3$, $YAlO_3$, and $YTiO_3$ were compared through the relation $a \approx b \approx \sqrt{2}a_p$ and $c \approx 2a_p$ ($a_p$: a pseudocubic subcell parameter). Consequently, the cell distortion factor, $d$ [Eq. (2)], was calculated from that sublattice parameters in the same pressure range,

$$d = \frac{\left[\left(\frac{a}{\sqrt{2}} - a_p\right)^2 + \left(\frac{b}{\sqrt{2}} - a_p\right)^2 + \left(\frac{c}{2} - a_p\right)^2\right]}{3a_p^2 \times 10^4}, \qquad (2)$$

where

$$a_p = \frac{\left(\frac{a}{\sqrt{2}} + \frac{b}{\sqrt{2}} + \frac{c}{2}\right)}{3},$$

obtaining a useful estimation of the departure from an ideal cubic model, for which $d$=0.[33]

Figure 7 shows the clear antithetic behavior of $YCrO_3$ and $YTiO_3$ with respect to $YAlO_3$ orthorhombic perovskite under pressure: while the orthochromate and the orthotitanate become more distorted and are characterized by an increase in the $d/d_0$ ratio, the orthoaluminate data describe an opposite trend characterized by a decreasing of the $d/d_0$ ratio toward a structure with higher symmetry. The slopes of the linear relationships in Fig. 7 inversely scale with room pressure $\langle B\text{-O-}B\rangle$ angles which in turn linearly decrease with increasing ionic radii of octahedral $B$ ions (i.e., slopes for $d/d_0$ vs $P$: $-0.0420_{YAlO3} < 0.0092_{YCrO3} < 0.0379_{YTiO3}$; $\langle B\text{-O-}B\rangle$: $152.2_{YAlO3} > 146.2_{YCrO3} > 140.8^{\circ}_{YTiO3}$; Shannon ionic radii of $^{VI}M^{3+}$ ions in $B$: $0.54_{Al} < 0.62_{Cr} < 0.67_{Ti}$ Å).[34] These trends suggest that the pressure-induced distortion of perovskite framework can be related to both the initial octahedral tilt angles and to the ionic radii of octahedral cations for 3:3 perovskites, irrespective of the difference in electron configuration of trivalent ions in $B$ sites. Based on this concept it can be predicted that a $YM^{3+}O_3$ perovskite with the ionic radius of $M^{3+}$ ion in the $B$ site equal to ~0.59 Å (e.g., $Ni^{3+}$ or $As^{3+}$), thus a $\langle B\text{-O-}B\rangle$ angle at room pressure around 147.4°, will exhibit, upon compression, a $d/d_0$ ratio close to 1.0 in the whole pressure range, meaning it will neither increase nor decrease its lattice distortion.

## IV. CONCLUDING REMARKS

The above considerations show that the contrasting evolution under pressure of $YCrO_3$ and $YTiO_3$ (increasing distortion) vs $YAlO_3$ (decreasing distortion) can be simply explained on the basis of the ionic radii of $B$ cations. In fact, the mesh size of the octahedral network is reduced in $YAlO_3$, as compared to $YCrO_3$ and $YTiO_3$, with the ionic size of $A$ cation (yttrium) remaining constant. As known from previ-

ous work,[9] the decrease in mean octahedral bond distance, $\langle B\text{-O}\rangle$, from $YCrO_3$ to $YAlO_3$ is accompanied by a shortening of the average $\langle A\text{-O}\rangle$ distance, with a net increase in the effective coordination number of Y in $YAlO_3$. This is also associated to a linear decrease in interoctahedral tilting and rotation angles from 152.9° and 151.1° in $YAlO_3$ to 146.7° and 145.7° in $YCrO_3$ at room pressure.[9] Conversely, the decrease in perovskite framework distortion upon increasing the *A* cation size, with the same cation in the *B* site, has been previously reported and discussed.[23,29] As illustrated in Fig. 8 (only $YAlO_3$ and $YCrO_3$ are sketched for the sake of simplicity), the more confined space of Y in $YAlO_3$ is responsible for the higher incompressibility of the *A* site compared to the *B* site in the orthoaluminate.[17]

The relatively larger shortening of the *B*-O bonds under pressure in $YAlO_3$ exerts an equivalent effect of the network mesh size reduction at room pressure, as discussed above, leading to a more regular structure of $YAlO_3$ at high pressures. The Y cation in $YCrO_3$ (and $YTiO_3$) does not exhibit the same strong confinement effect as in $YAlO_3$ where the *A* site is easier to compress and does not hamper the increase in octahedral tilting and rotation in $YCrO_3$ and $YTiO_3$ at high pressures.

These considerations confirm that the pressure-induced distortion of perovskite lattice is primarily controlled by the compressibility ratio of the *B* and *A* sites ($\beta_B/\beta_A$), in agreement to what suggested by several authors.[35] However, the general rule which models $\beta_B/\beta_A$ through the ratio of the bond valence difference parameters ($M_A/M_B$) calculated for the *A* and *B* polyhedra (i.e., $\beta_B/\beta_A = M_A/M_B$) (Ref. 18) fails to predict the increasing distortion of both $YCrO_3$ and $YTiO_3$. As a consequence, either the $\beta_B/\beta_A$ ratio cannot be accurately estimated from bond valence calculations or the assumption that $M_A/M_B = 1.0$ is the boundary between perovskites evolving under pressure to higher symmetry ($M_A/M_B > 1.0$) or to lower symmetry ($M_A/M_B < 1.0$) structures is not valid.

## ACKNOWLEDGMENTS

Access to ID27 beamline at the European Synchrotron Radiation Facility (ESRF) was provided under the public beamtime program (exp. no. HS3936). We thank Michael Hanfland (ESRF) for advice and technical support.

*Author to whom correspondence should be addressed; cru@unife.it

[1] R. Mitchell, *Perovskites: Modern and Ancient* (Almaz Press, Ontario, 2002).
[2] A. Navrotsky and D. Weidner, *Perovskite: A Structure of Great Interest to Geophysics and Materials Science*, Geophysical Monograph Vol. 45 (AGU, Washington, DC, 1989).
[3] T. Ishihara, *Perovskite Oxide for Solid Oxide Fuel Cells*, Fuel Cells and Hydrogen Energy Series (Springer, New York, 2009).
[4] T. Wolfram and S. Ellialtioglu, *Electronic and Optical Properties of d-Band Perovskites* (Cambridge University Press, Cambridge, England, 2006).
[5] S. Wang, B. Lin, Y. Dong, D. Fang, H. Ding, X. Liu, and G. Meng, J. Power Sources **188**, 483 (2009).
[6] G. Carini II, H. Anderson, M. Nasrallah, and D. Sparlin, J. Solid State Chem. **94**, 329 (1991).
[7] C. R. Serrao, A. K. Kundu, S. B. Krupanidhi, U. V. Waghmare, and C. N. R. Rao, Phys. Rev. B **72**, 220101 (2005).
[8] K. Ramesha, A. Llobet, Th. Proffen, C. Serrao, and C. Rao, J. Phys.: Condens. Matter **19**, 102202 (2007).
[9] G. Cruciani, M. Ardit, M. Dondi, F. Matteucci, M. Blosi, M. C. Dalconi, and S. Albonetti, J. Phys. Chem. A **113**, 13772 (2009).
[10] P. Bouvier and J. Kreisel, J. Phys.: Condens. Matter **14**, 3981 (2002).
[11] K. Knight, W. Marshall, N. Bonanos, and D. Francis, J. Alloys Compd. **394**, 131 (2005).
[12] M. Lufaso, S. Mugavero III, W Gemmill, Y. Lee, T. Vogt, and H.-C. zur Loye, J. Alloys Compd. **433**, 91 (2007).
[13] N. Ross, Phys. Chem. Miner. **25**, 597 (1998).
[14] N. Ross and R. Angel, Am. Mineral. **84**, 277 (1999).
[15] N. Ross and T. Chaplin, J. Solid State Chem. **172**, 123 (2003).
[16] N. Ross, J. Zhao, J. Burt, and T. Chaplin, J. Phys.: Condens. Matter **16**, 5721 (2004).
[17] N. Ross, J. Zhao, and R. Angel, J. Solid State Chem. **177**, 1276 (2004).
[18] R. J. Angel, J. Zhao, and N. L. Ross, Phys. Rev. Lett. **95**, 025503 (2005).
[19] J. Zhao, N. Ross, and R. Angel, Acta Crystallogr., Sect. B: Struct. Sci. **62**, 431 (2006).
[20] I. Loa, P. Adler, A. Grzechnik, K. Syassen, U. Schwarz, M. Hanfland, G. K. Rozenberg, P. Gorodetsky, and M. P. Pasternak, Phys. Rev. Lett. **87**, 125501 (2001).
[21] I. Loa, X. Wang, K. Syassen, H. Roth, T. Lorenz, M. Hanfland, and Y.-L. Mathis, J. Phys.: Condens. Matter **19**, 406223 (2007).
[22] M. Sugahara, A. Yoshiasa, Y. Komatsu, T. Yamanaka, N. Bolfan-Casanova, A. Nakatsuka, S. Sasaki, and M. Tanaka, Am. Mineral. **91**, 533 (2006).
[23] X. Wu, S. Qin, and Z. Wu, J. Phys.: Condens. Matter **18**, 3907 (2006).
[24] M. Mezouar, W. Crichton, S. Bauchau, F. Thurel, H. Witsch, F. Torrecillas, G. Blattmann, P. Marion, Y. Dabin, J. Chavanne, O. Hignette, C. Morawe, and C. Borel, J. Synchrotron Radiat. **12**, 659 (2005).
[25] A. Hammersley, S. Svensson, M. Hanfland, A. Fitch, and D. Hausermann, High Press. Res. **14**, 235 (1996).
[26] R. Forman, G. Piermarini, J. Barnett, and S. Block, Science **176**, 284 (1972).
[27] A. Larson and R. Von Dreele, Los Alamos National Laboratory Report No. LAUR 86–748, 2004 (unpublished).
[28] H. Toby, J. Appl. Crystallogr. **34**, 210 (2001).
[29] G. Cruciani, F. Matteucci, M. Dondi, G. Baldi, and A. Barzanti, Z. Kristallogr. **220**, 930 (2005).
[30] S. Geller and A. Wood, Acta Crystallogr. **9**, 563 (1956).

[31] I. Brown and D. Altermatt, Acta Crystallogr., Sect. B: Struct. Sci. **41**, 244 (1985).

[32] R. Angel, in *High-Pressure, High Temperature Crystal Chemistry*, Reviews in Mineralogy and Geochemistry Vol. 41, edited by R. Hazen and R. Downs (MSA, Washington, DC, 2000).

[33] S. Sasaki, C. Prewitt, and R. Liebermann, Am. Mineral. **68**, 1189 (1983).

[34] R. Shannon, Acta Crystallogr., Sect. A: Cryst. Phys., Diffr., Theor. Gen. Crystallogr. **32**, 751 (1976).

[35] D. Andrault and J. Poirier, Phys. Chem. Miner. **18**, 91 (1991).